Supplement of Atmos. Chem. Phys., 20, 12983–12993, 2020
https://doi.org/10.5194/acp-20-12983-2020-supplement

Atmospheric Chemistry and Physics
Open Access
EGU

Supplement of

Kinetics of dimethyl sulfide (DMS) reactions with isoprene-derived Criegee intermediates studied with direct UV absorption

Mei-Tsan Kuo et al.

Correspondence to: Jim Jr-Min Lin (jimlin@gate.sinica.edu.tw)

S1 Summary of the experimental conditions and results

Table S1. Summary of the experimental conditions and results for the reaction CH_2OO+DMS at 308 nm photolysis. T = 296.8–297.2 K; $[O_2] = (3.28–3.32)\times10^{17}$ cm^{-3}; P_{total} = 299.9–301.5 Torr.

Exp#	$[CH_2I_2]$ /10^{13} cm^{-3}	I_{308nm} /mJ cm^{-2}	k_0 /s^{-1}	k_{DMS} /10^{-16} cm^3 s^{-1}
1	16.1	1.19	232±2[a]	7.8±4.1[a]
2	16.3	2.35	464±3	10.9±5.6
3	16.2	3.63	698±3	22.0±5.5
4	16.5	4.83	956±5	–4.1±10.4
5	12.6	0.34	54±2	9.1±4.5
6	21.2	0.31	79±2	10.2±4.1
7	20.7	0.31	90±2	8.6±4.9
8	21.1	0.74	188±1	–3.2±1.7
9	19.6	0.95	240±2	12.0±3.5
10	2.30	9.97	261±8	28.7±16.7
11	25.4	2.27	680±4	24.1±8.2
			average	11.5
			standard deviation[b]	10.3

[a] Averaged value ± 1 sigma error of the mean (statistical only, not including systematic errors). Note: 1 sigma error of the mean = standard deviation / sqrt(degrees of freedom)

[b] Standard deviation of the 11 data points of k_{DMS}.

Table S2. Summary of the experimental conditions and results for the reaction CH_2OO+DMS at 248 nm photolysis. T = 296.7K–296.8 K; $[O_2] = 3.29\times10^{17}$ cm^{-3}; P_{total} = 299.5–299.7 Torr.

Exp#	$[CH_2I_2]$ /10^{13} cm^{-3}	I_{248nm} /mJ cm^{-2}	k_0 /s^{-1}	k_{DMS} /10^{-16} cm^3 s^{-1}
12	19.3	1.10	109±1[a]	16.2±10.3[a]
13	19.0	2.18	197±1	25.5±8.6
14	18.9	3.17	275±1	31.6±11.5
			average	24.4
			standard deviation[b]	7.8

[a] Averaged value ± 1 sigma error of the mean (statistical only, not including systematic errors). Note: 1 sigma error of the mean = standard deviation / sqrt(degrees of freedom)

[b] Standard deviation of the 3 data points of k_{DMS}.

Table S3. Summary of the experimental conditions and results for the reaction MVKO + DMS at 248 nm photolysis. T = 297.0–298.1 K; $[O_2]$ = (3.28–3.41)×10^{17} cm^{-3}.

Exp#	Precursor *Abs*[b]	P_{total} /Torr	I_{248nm} /mJ cm^{-2}	k_r /s^{-1}	adduct yield $1-\alpha$[a] /%	k_0 /s^{-1}	k_{DMS} /10^{-16} cm^3 s^{-1}
15	0.100	301.4	1.09	1182±14[b]	91.8±0.3[c]	115±2[b]	116.5±34.3[b]
16	0.220	303.0	1.06	1442±7	89.2±0.1	151±2	94.7±34.5
17	0.331	301.6	1.03	1641±5	87.2±0.1	182±2	73.2±24.0
18	0.334	301.9	0.58	1386±10	90.4±0.2	140±1	99.9±19.1
19	0.056	302.1	1.25	1033±48	91.1±1.6	123±8	75.0±70.7
20	0.151	302.2	1.23	1109±14	91.2±0.3	131±2	44.2±22.5
21	0.057	302.5	2.45	1203±14	90.6±0.2	146±2	19.6±17.0
22	0.158	302.3	2.43	1395±6	87.0±0.1	179±5	78.7±56.1
23	0.056	302.3	3.72	1330±5	88.9±0.3	229±2	33.2±15.9
24	0.160	302.4	3.67	1652±8	84.0±0.1	274±1	–15.0±16.7
25	0.179	30.6	1.19	1297±7	57.0±0.2	138±2	70.3±58.1
26	0.558	30.2	1.14	2123±19	49.2±0.1	255±2	67.8±59.3
27	0.289	100.2	1.18	1481±12	79.2±0.2	153±1	68.4±7.7
28	0.746	99.9	1.11	2146±8	70.7±0.1	321±2	39.6±25.8
29	0.142	299.5	1.19	1362±11	88.7±0.1	126±1	57.1±14.8
					average		61.6
					standard deviation[d]		33.4

[a] The yield of $CH_3(C_2H_3)CIOO$.

[b] The estimated absorbance of the precursor (1,3-diiodo-2-butene) at 238 nm in the photolysis reactor (using L = 426 cm).

[c] Averaged value ± 1 sigma error of the mean (statistical only, not including systematic errors). The actual error bar would be larger since k_r is highly correlated with other fitting parameters like $(1-\alpha)$. Lin et al. have used SO_2 scavenger to obtain more robust results for k_r (Lin et al., 2020).

[d] Standard deviation of the 15 data points of k_{DMS}.

S2 Observed decay rate coefficient of CH_2OO at various conditions

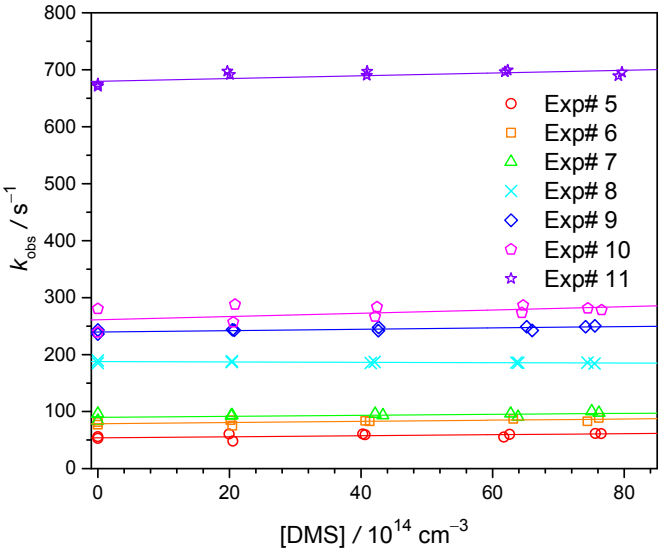

Fig. S1. First-order decay rate coefficient of CH_2OO, k_{obs}, against [DMS] at various experimental conditions (Exp#5–11, Table S1). The wavelength of the photolysis laser is 308 nm. For each data point, the error of the single exponential fitting is lees than 1% (thus not shown).

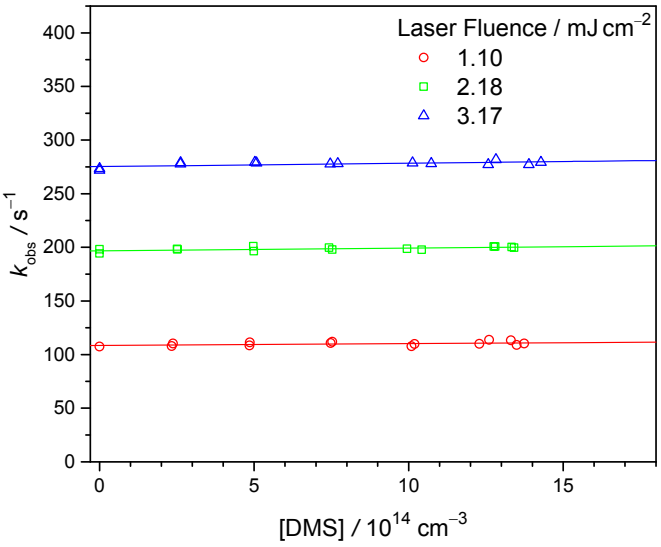

Fig. S2. First-order decay rate coefficient of CH_2OO, k_{obs}, against [DMS] at various photolysis laser fluence (Exp#12–14, Table S2). The wavelength of the photolysis laser is 248 nm. For each data point, the error of the single exponential fitting is lees than 1% (thus not shown).

S3 Kinetic model for MVKO reactions

To obtain more quantitative values for k_{DMS}, we performed kinetic analysis with the following model. At t = 0, the precursor ICH_2-CH=C(I)-CH_3 is photodissociated into $CH_3(C_2H_3)CI$ + I. Under the high $[O_2]$ conditions (~3.3×10^{17} cm^{-3}) in our experiment, the reactions of $CH_3(C_2H_3)CI + O_2$ (R3a) and (R3b) proceed within a very short time (< 0.1 ms). However, different from the case of CH_2OO, an additional MVKO signal rises slowly until about 2 ms (R3c), followed by a decay in longer reaction times (due to (R4) and (R5)). The formation/decomposition of the adduct of MVKO and I atom (R3b)/(R3c) are pressure dependent.

$CH_3(C_2H_3)CI + O_2 \rightarrow I + CH_3(C_2H_3)COO$ (MVKO) (R3a; αk_{O2})

$CH_3(C_2H_3)CI + O_2 + M \rightarrow CH_3(C_2H_3)CIOO + M$ (R3b; $(1-\alpha)k_{O2}$)

$CH_3(C_2H_3)CIOO + M \rightarrow I + CH_3(C_2H_3)COO + M$ (R3c; k_r)

$CH_3(C_2H_3)COO$ (MVKO) + DMS $\rightarrow$ Products (R4; k_{DMS})

$CH_3(C_2H_3)COO$ (MVKO) + X (radicals) $\rightarrow$ Products (R5; k_X)

The detail kinetics of the adduct decomposition into MVKO + I will be published elsewhere. In brief, MVKO is either formed directly (R3a), or via the formation and consecutive decomposition of an adduct of $CH_3(C_2H_3)CIOO$ ((R3b) and (R3c)). From the differential rate equations of these three reactions, the following analytical expression for [MVKO](t) can be derived:

$$\begin{aligned}[\mathrm{MVKO}](t) &= [\mathrm{MVKO}]_0 e^{-k_{\mathrm{obs}}t} + [\mathrm{adduct}]_0 \frac{k_r}{k_r - k_{\mathrm{obs}}}[e^{-k_{\mathrm{obs}}t} - e^{-k_r t}] \\ &= [\mathrm{MVKO}]_{\mathrm{total}}\{\alpha e^{-k_{\mathrm{obs}}t} + (1-\alpha)\frac{k_r}{k_r - k_{\mathrm{obs}}}[e^{-k_{\mathrm{obs}}t} - e^{-k_r t}]\}\end{aligned} \quad (3)$$

with α and $(1-\alpha)$ as the yields of the prompt MVKO and the adduct ($[MVKO]_{total}$ = $[MVKO]_0$ + $[adduct]_0$) and $k_{obs} = k_0 + k_{DMS}[DMS]$ as in the case of CH_2OO. Fitting this equation to the measured absorbance–time profiles treating k_{obs}, k_r, and α as variable parameters, we obtained k_{obs}. Selected results of k_{obs} are presented in Figure 4 and all results are summarized in Table S3.

S4 Observed decay rate coefficient of MVKO at various conditions

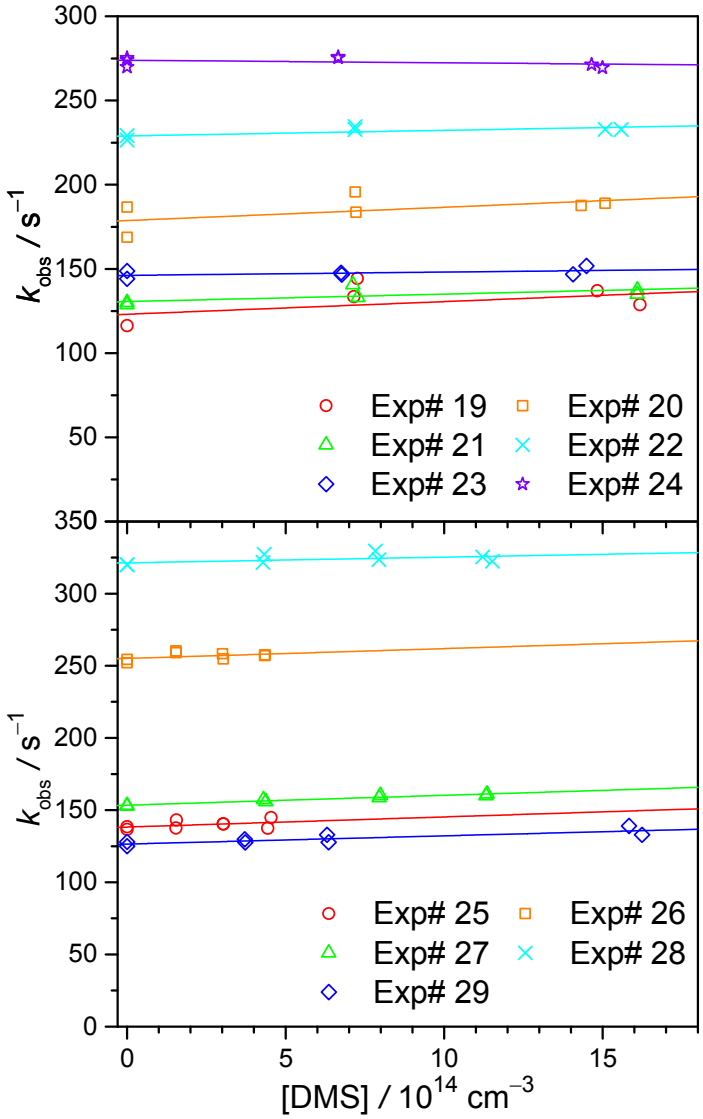

Fig. S3. First-order decay rate coefficient of MVKO, k_{obs}, against [DMS] at various experimental conditions (Exp#19–29). The wavelength of the photolysis laser is 248 nm.

S5 Effect of DMS photolysis

Assuming the photolysis yield of DMS is unity, the concentration of the photodissociated DMS, $[DMS]_{diss}$, can be deduced from the following equation:

$$[DMS]_{diss} = [DMS]\rho\sigma$$

$$\rho = I\frac{\lambda}{hc}$$

where $\rho = I\lambda/hc$ is the number of photons per unit area and σ is the reported absorption cross section of DMS(Limão-Vieira et al., 2002); I and λ are the fluence and wavelength of the photolysis laser; h and c are the Planck constant and speed of light, respectively. The maximum values of photodissociated DMS and CH_2I_2 precursor are estimated as in Table S4.

Table S4. Estimation for the photodissociated DMS and CH_2I_2.

Wavelength	I / mJ cm^{-2}	ρ / cm^{-2}	σ / cm^2	$[DMS]_{diss}/[DMS]$	[DMS] /cm^{-3}	$[DMS]_{diss}$ /cm^{-3}
248 nm	3.72	4.64×10^{15}	1.28×10^{-20}	5.9×10^{-5}	1.7×10^{15}	1.0×10^{11}
308 nm	9.97	1.55×10^{16}	$<1\times10^{-22}$	$<1.5\times10^{-6}$	8.1×10^{15}	$<1.3\times10^{10}$

				$[CH_2I_2]_{diss}/[CH_2I_2]$	$[CH_2I_2]$ /cm^{-3}	$[CH_2I_2]_{diss}$ /cm^{-3}
248 nm	3.17	3.96×10^{15}	1.6×10^{-18}	6.3×10^{-3}	1.9×10^{14}	1.2×10^{12}
308 nm	9.97	1.55×10^{16}	3.3×10^{-18}	5.1×10^{-2}	2.3×10^{13}	1.2×10^{12}

High $[DMS]_{diss}$ at 248 nm photolysis would generate radical products, which may react with CH_2OO or MVKO and may absorb light at our probe wavelength (see **Figure S4**). On the other hand, the very minor $[DMS]_{diss}$ at 308 nm photolysis would not cause a problem. Hence, at 248 nm photolysis, we limit [DMS] ≤ 1.7×10^{15} cm^{-3} and I_{248nm} ≤ 3.72 mJ cm^{-2} (Exp#23–24) to constraint $[DMS]_{diss}$ ≤ 1.0×10^{11} cm^{-3}. **Figure S5** shows the background trace at 248 nm photolysis with constraint [DMS] and I_{248nm}. No significant background due to $[DMS]_{diss}$ is observed, except absorption caused from the optics. Besides, in **Figure S9**, we can see that the results of CH_2OO+DMS reaction at 248 nm photolysis are quite similar to those at 308 nm, while a slightly higher k_{DMS} can be observed for 248 nm at high $I_{248\ nm}$, indicating that $[DMS]_{diss}$ only has a minor effect.

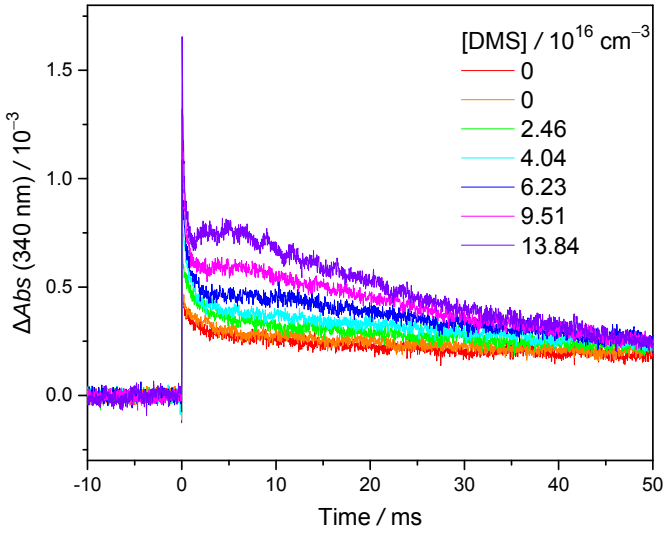

Fig. S4. Background traces recorded under extra-high [DMS]. The traces were obtained with 248 nm photolysis laser (I_{248nm} = 3.34 mJ cm^{-2}). The experimental conditions are : P_{total} =297.2 Torr, [O_2] =3.23 ×10^{17} cm^{-3}, T=299 K. The length of the cell for monitoring [DMS] is 1 cm. The photolysis laser pulse defines t = 0. The absorbance change under zero [DMS] comes from the interaction of the optics and the photolysis laser pulse, whereas the "spike" near time zero may come from the absorption of the radical products of DMS photolysis, likely CH_3S (Liu et al., 2005) and/or vibrationally excited CH_3S. Note that in the kinetic experiments, the used [DMS] was much lower (< 1.7×10^{15} cm^{-3}) such that the background did not depend on [DMS] (see Figure S5).

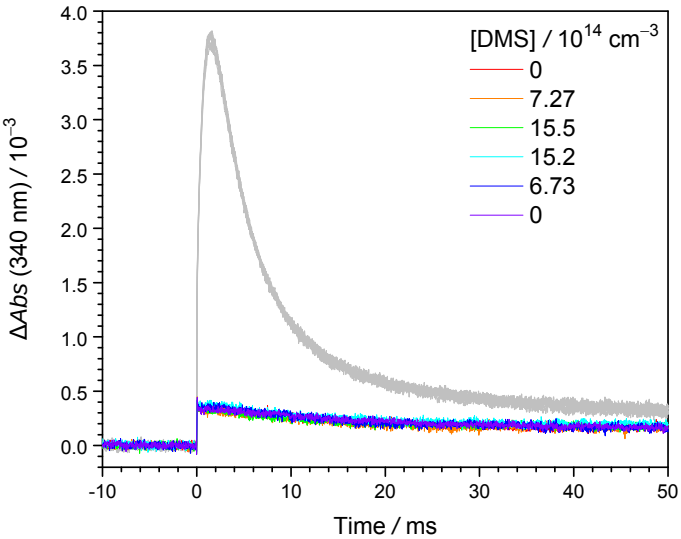

Fig. S5. Background traces under normal DMS concentrations, represented in colour lines, and the raw signal traces (without background subtraction), represented in grey lines,

obtained with 248 nm photolysis laser (I_{248nm} = 2.43 mJ cm^{-2}). See Exp#22 of Table S3 for the experimental conditions.

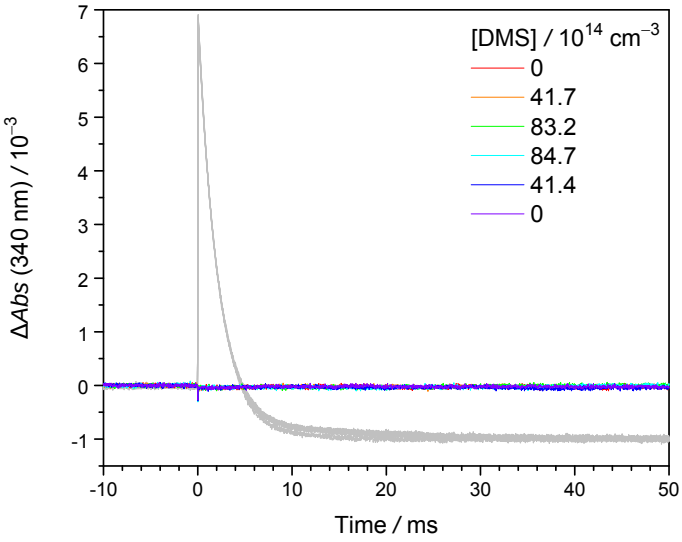

Fig. S6. Background traces under normal DMS concentrations, represented in colour lines, and the raw signal traces (without background subtraction), represented in grey lines, obtained with 308 nm photolysis laser (I_{308nm} = 2.35 mJ cm^{-2}). See Exp#2 of Table S1 for the experimental condition. Note that the optics (longpass filters) are different from those at 248 nm.

S6 Dependence of k_0 ,k_{DMS} , and k_r on laser fluence and precursor concentration

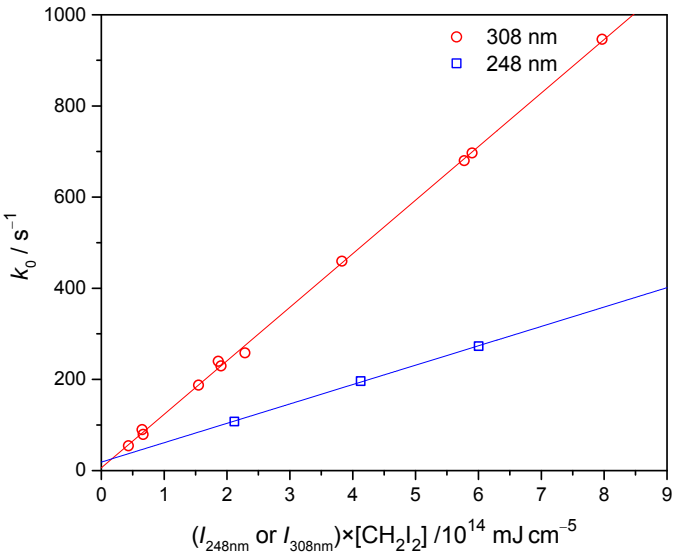

Fig. S7. Plot of k_0 against the product of the laser fluence (I_{248nm} or I_{308nm}) and the precursor concentration [CH_2I_2] for the experiments (Exp#1–14, Tables S1–S2) of CH_2OO+DMS reaction. The x-axis essentially represents the total amounts of radical species generated through the photolysis of the precursor (R1) and the subsequent reactions (R2). Higher radical concentration results in faster CH_2OO decay, thus higher k_0. The difference of the slopes mainly comes from the difference of CH_2I_2 absorption cross sections at these two wavelengths (see Table S4). The main loss processes of CH_2OO are reactions with radical byproducts like iodine atoms and its self-reaction. The observed values of k_0 (e.g., 232 s^{-1} for Exp#1) are consistent with the values (e.g., 180 s^{-1} at the condition of Exp#1) that are estimated using the reported kinetic data (yield and rate coefficients)(Mir et al., 2020; Ting et al., 2014). Note that there are experiments having different combinations of [CH_2I_2] and I_{308nm}, but very similar I_{308nm}×[CH_2I_2] (like Exp#3,11; Exp#1,9).

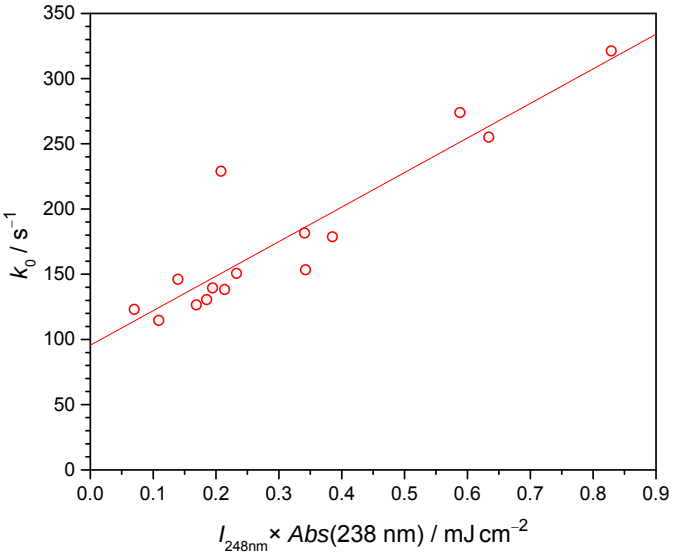

Fig. S8. As Figure S7, but for the experiments (Exp#15–29) of MVKO+DMS reaction. Because the absorption cross section of the precursor (1,3-diiodo-2-butene) is not available, we use the absorbance at 238 nm in the reactor (using L = 426 cm) to represent the concentration.

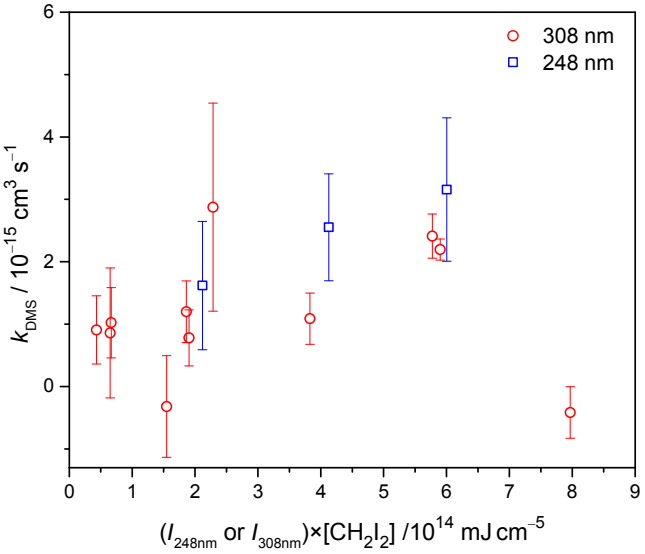

Fig. S9. Plot of k_{DMS} against the product of the laser fluence (I_{248nm} or I_{308nm}) and the precursor concentration [CH_2I_2] for the experiments (Exp#1–14, Tables S1–S2) of CH_2OO+DMS reaction. The x-axis essentially represents the total amounts of radical species generated through the photolysis of the precursor (R1) and the subsequent reactions (R2). No observable trend of k_{DMS} can be found for the data of 308 nm photolysis, whereas k_{DMS} at 248 nm photolysis increases as I_{248nm}x[CH_2I_2] increases, which may result from the increased

radical generation from the DMS photolysis. Note that there are experiments having different combinations of $[CH_2I_2]$ and I_{308nm}, but very similar I_{308nm}x$[CH_2I_2]$ (like Exp#3,11; Exp#1,9).

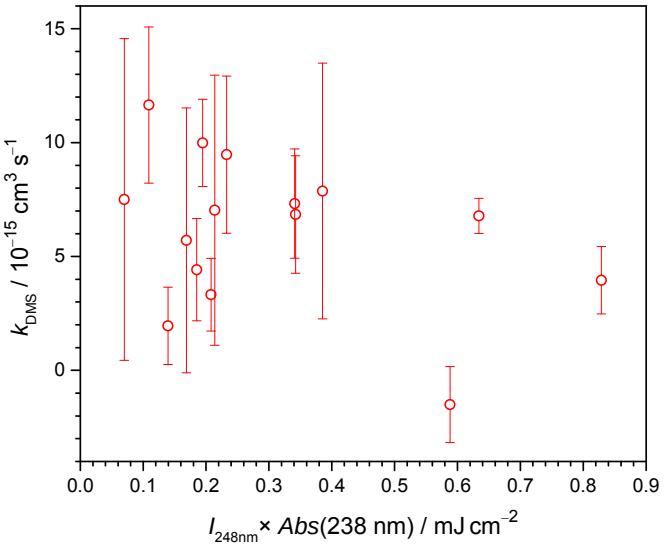

Fig. S10. As Figure S9, but for k_{DMS} in Exp#15–29 of MVKO+DMS reaction. No significant trend for k_{DMS} is observed. Because the absorption cross section of the precursor (1,3-diiodo-2-butene) is not available, we use the absorbance at 238 nm in the reactor (using L = 426 cm) to represent the concentration.

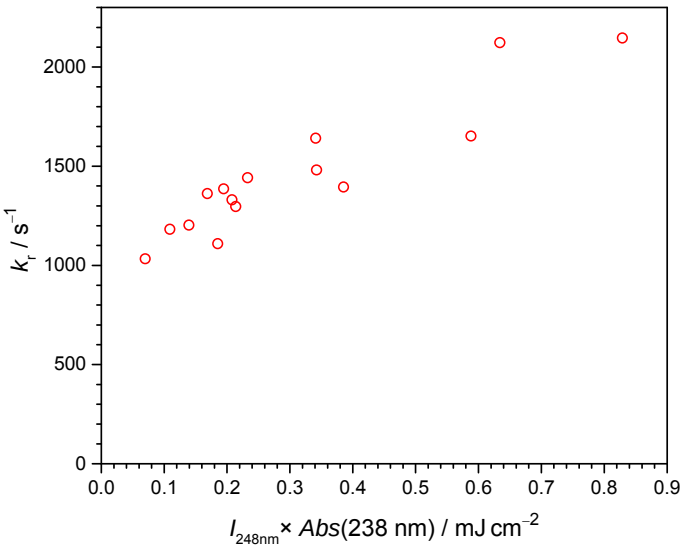

Fig. S11. Plot of k_r against the product of the laser fluence (I_{248nm}) and the absorbance of 1,3-diiodo-2-butene at 238 nm in the photolysis cell (*Abs*(238nm)) for the experiments of MVKO+DMS reaction (Exp#15–29, Tables S3). The x-axis essentially represents the total amounts of radical species generated through the photolysis of the precursor (R1) and the subsequent reactions (R2). Higher radical concentration results in faster decay of the adduct, thus higher k_r. Because the absorption cross section of the precursor (1,3-diiodo-2-butene) is not available, we use the absorbance at 238 nm in the reactor (using L = 426 cm) to represent the concentration.

S7 Representative time traces for the CH_2OO+DMS reaction obtained with 308 nm photolysis

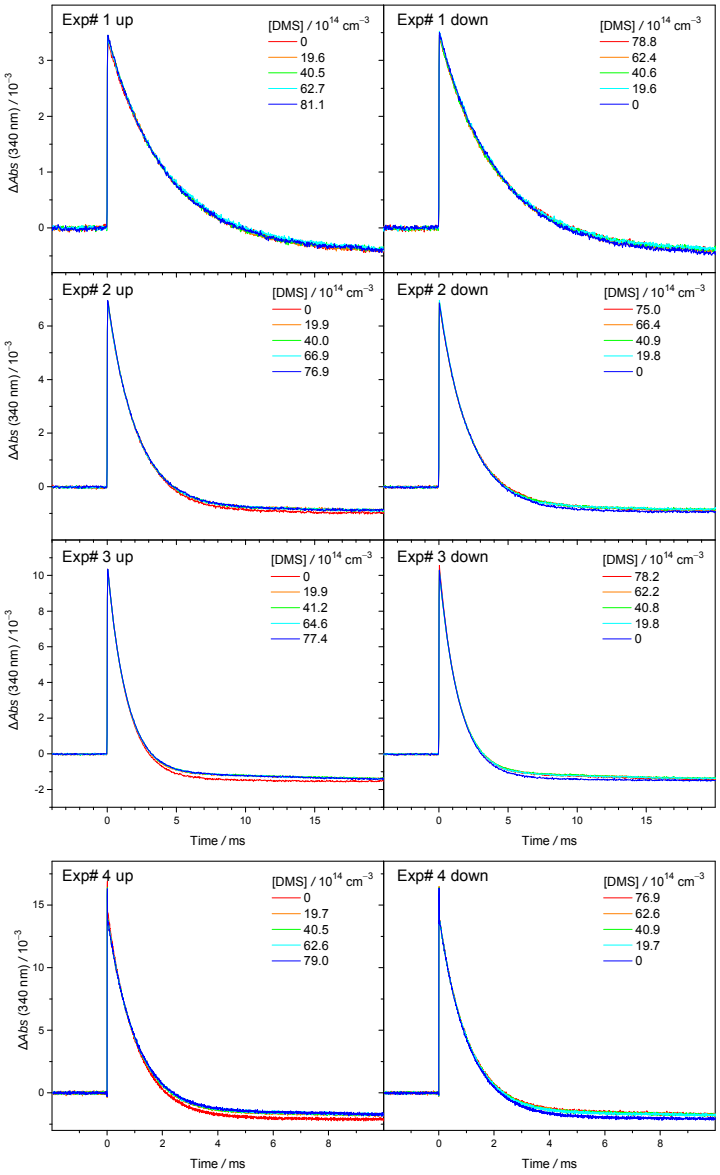

Fig. S12. Representative time traces of CH_2OO absorption at 340±5nm at various [DMS] (Exp#1–4). The wavelength of the photolysis laser was 308 nm and the laser pulse is set at the time zero. In each experiment, [DMS] was scanned from 0 to the maximum (labeled as "up"), and scanned from maximum to 0 (labeled as "down"). The negative baseline is resulted from the depletion of the precursor CH_2I_2.

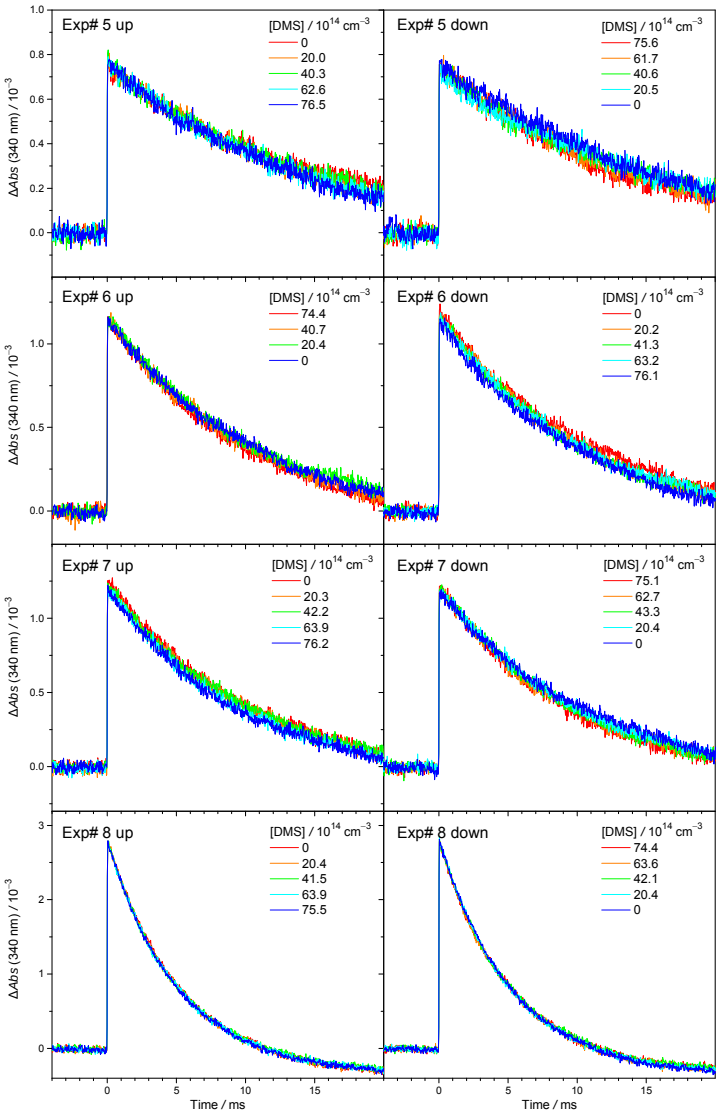

Fig. S13. As Fig. S12, but different experiment sets (Exp#5–8).

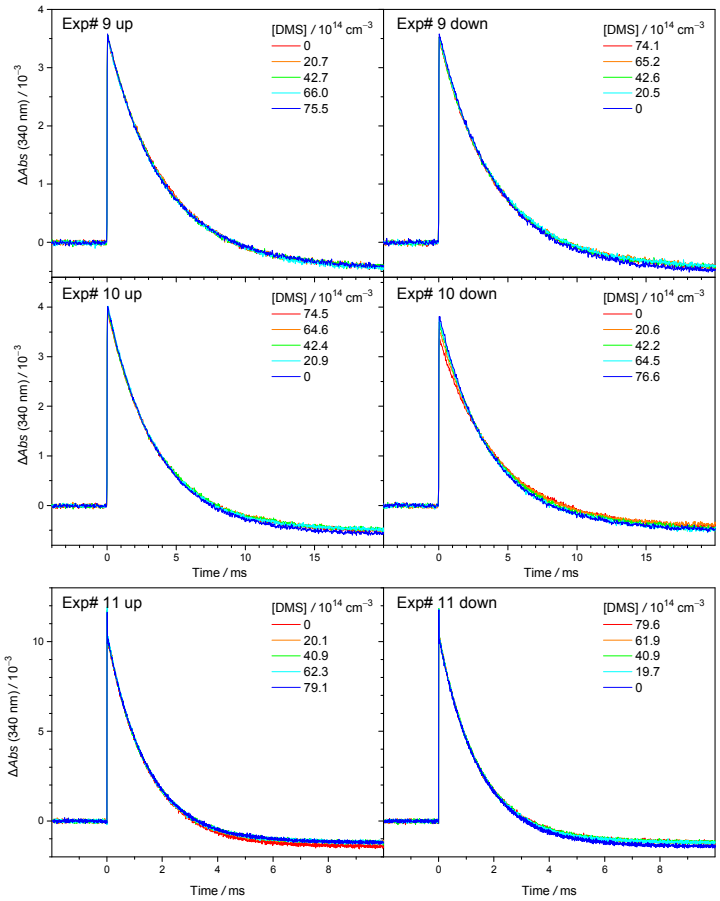

Fig. S14. As Fig. S12, but different experiment sets (Exp#9–11).

S8 Representative time traces for the CH_2OO+DMS reaction obtained with 248 nm photolysis

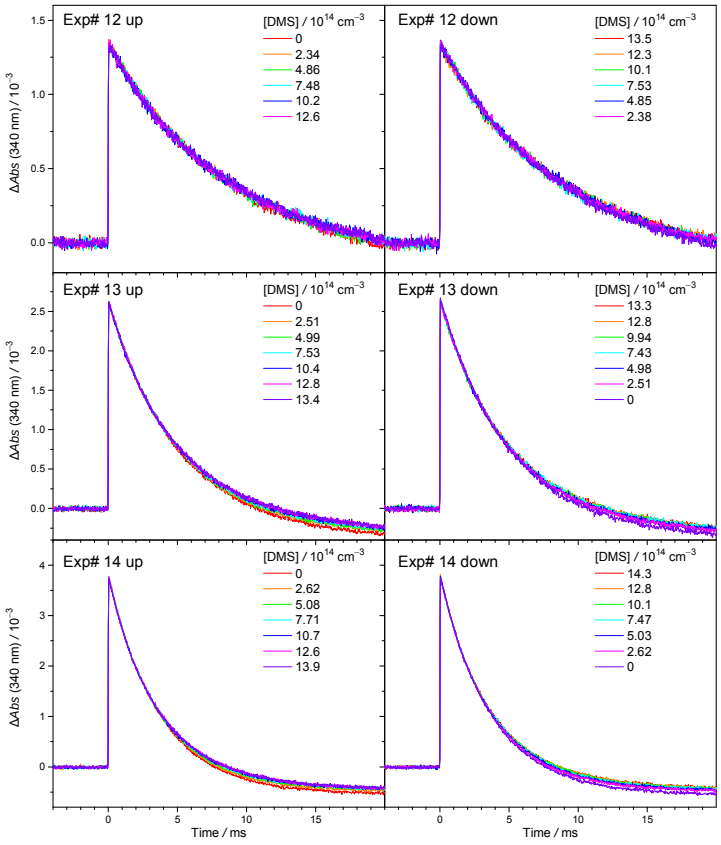

Fig. S15. Representative time traces of CH_2OO at 340±5nm at various [DMS] (Exp# 12–14). The wavelength of the photolysis laser was 248 nm and the laser pulse is set at the time zero. In each experiment, [DMS] was scanned from 0 to the maximum (labeled as "up"), and scanned from maximum to 0 (labeled as "down"). The negative baseline resulted from the depletion of the precursor CH_2I_2.

S9 Representative time traces for the MVKO+DMS reaction obtained with 248 nm photolysis

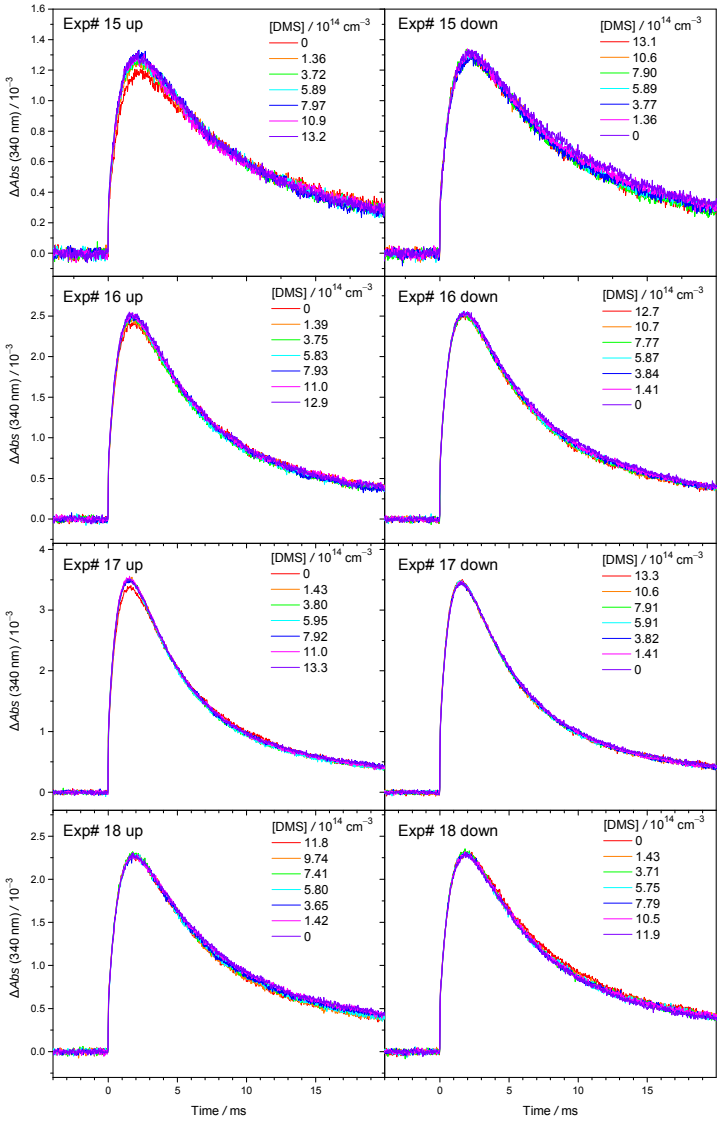

Fig. S16. Representative time traces of MVKO at 340±5nm at various [DMS] (Exp#15−18). The wavelength of the photolysis laser was 248 nm and the laser pulse is set at the time zero. In each experiment, [DMS] was scanned from 0 to the maximum (labeled as “up”), and scanned from maximum to 0 (labeled as “down”).

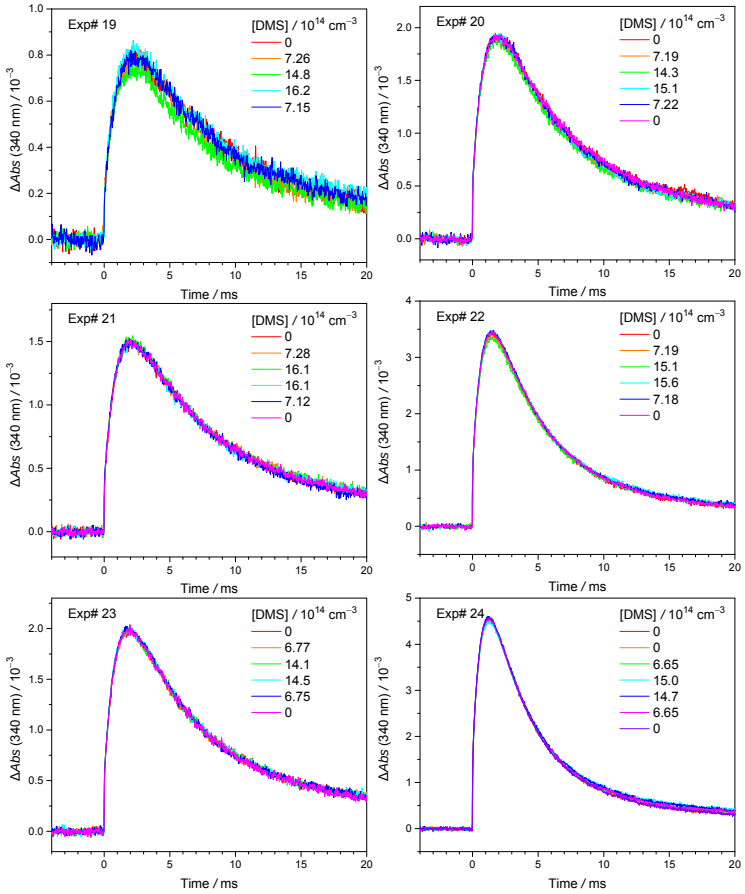

Fig. S17. Representative time traces of MVKO at 340±5nm at various [DMS] (Exp#19–24). The wavelength of the photolysis laser was 248 nm and the laser pulse is set at the time zero.

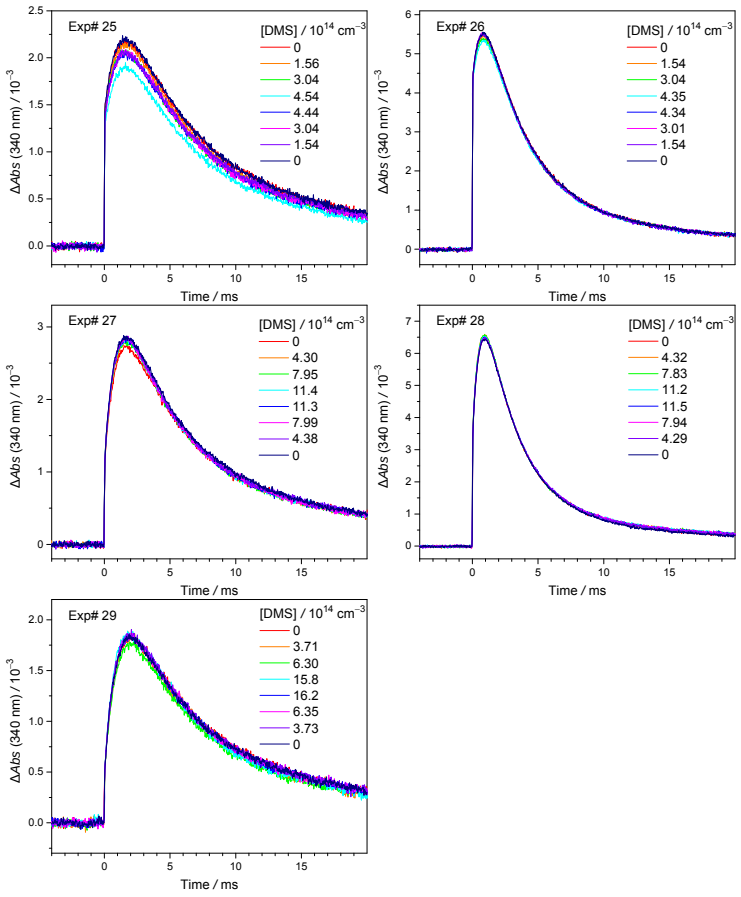

Fig. S18. As Fig. S17, but different experiment sets (Exp#25–29).

S10 Computational details for the reaction of CH_2OO + DMS

Additional methodological information

The CH_2OO + DMS system was characterized at the CCSD(T)/aug-cc-pVTZ//M06-2X/aug-cc-pV(T+d)Z level of theory. Though the computational demands of the reaction system prevent us from doing higher-level calculations at this time, this level of theory is expected to be sufficient to give a good idea of the PES layout, and derive rate coefficients with an accuracy of about one to two orders of magnitude. In particular, the study by Newland et al. proposes a very fast reaction which should then have a low energy barrier (Newland et al., 2015), whereas the current experimental study finds very slow elementary reactions which perforce must have a high energy barrier. The level of theory applied is able to easily discriminate between these extreme cases.

An additional set of exploratory calculations were performed at the M06-2X/cc-pVDZ level of theory, specifically on DMS + larger CI, DMS + CH_2OO in the presence of O_2, and unimolecular reactions of CH_2OO, *syn*-CH_3CHOO, *anti*-CH_3CHOO, and *cyc*-$CH_2OOS(O)O$- with and without complexation with DMS. These calculations at lower level are discussed here in the supporting information. For these calculations, only relative barrier heights on analogous reactions are important, which are sufficiently well described at the level of theory employed. As no indication for a significant enhancing effect on the reaction rate was found, no attempt was made to improve the absolute barrier height predictions.

Impact of substitutions of the CI, or the presence of O_2, on the CI + DMS reaction

Calculations for CH_2OO + DMS + O_2 reveal no influence of O_2 as a reaction partner, though the $(CH_3)_2SCH_2OO$ adduct may form a complex with O_2 stabilized by few kcal mol^{-1}. O_2 addition on the $(CH_3)_2SCH_2OO$ and $CH_3S(=CH_2)CH_2OOH$ adducts, forming triplet peroxy radicals, was found to have large barriers exceeding 15 kcal mol^{-1}, and is not competitive against redissociation of the CI+DMS adducts even at atmospheric O_2 concentrations.

Calculations on the reactions of *syn*-CH_3CHOO and *anti*-CH_3CHOO with DMS show that, as opposed to the CH_2OO case, formation of $(CH_3)_2SCH(CH_3)OO$ adducts is endothermic by a few kcal mol^{-1}, making reaction of substituted CI with DMS even less favorable. Finally, for all conformers of MVKO, the adduct with DMS was even found to be unstable at the M06-2X/cc-pVDZ level of theory: the needed C−S bond in the adduct appears to be too weak to compensate for the loss of conjugation stabilization in MVKO, and the system reverts to the MVKO + DMS complex instead, without a formal C−S bond. As a result, the barrier for the migration of a DMS methyl H-atom to the carbonyl oxide oxygen to form a methylidene adduct is ~10 kcal/mol higher than for the analogous TS in the CH_2OO+DMS system which does feature a weakly bonded intermediate adduct. The direct oxygen transfer from *E*- or *Z*-MVKO to DMS, forming MVK + DMSO, was found to have a similarly high energy barrier as in the CH_2OO+DMS system. No viable reaction channels were found

involving the double bond in MVKO. The lack of accessible transition states then prohibits rapid direct reaction between DMS and MVKO.

DMS as a catalyst

The experiments of Newland et al. found no evidence of DMS consumption (Newland et al., 2015), suggesting that the DMS activity hampering SO_2 oxidation by CI in their isoprene + O_3 system might be caused by catalytic effects. Hence, we examined whether the unimolecular decay of CI could be affected by complexation with DMS, performing a set of calculations using the lower level M06-2X/cc-pVDZ level of theory. At that level of theory, the complexes of CH_2OO, *syn*-CH_3CHOO and *anti*-CH_3CHOO with DMS are stabilized by 8.5 to 10.9 kcal mol^{-1} (likely overestimated due to basis set superposition errors). The barriers for dioxirane formation in CH_2OO, *syn*-CH_3CHOO and *anti*-CH_3CHOO are 22.0, 25.8 and 18.4 kcal mol^{-1} without DMS, respectively, while in the DMS complex they are 24.1, 26.8 and 20.4 kcal mol^{-1} above the complex, respectively. In *syn*-CH_3CHOO, the energy barrier for 1,4-H-migration (vinylhydroperoxide channel) without and with DMS are 12.7 and 15.8 kcal mol^{-1}, respectively, again calculated from the bottom of the CI-DMS complex. The dominant unimolecular reaction of *E*-MVKO is a 1,4-H-shift (VHP-channel), where at the M06-2X/cc-pVDZ level of theory, we find similar results as for the methylated CH_3CHOO, i.e. the barrier height without (12.1 kcal/mol) and with complexing DMS (14.2 kcal/mol from the ground state of the complex) are essentially identical (see Table S5). For *Z*-MVKO, the dominant unimolecular reaction is a 5-membered ring closure, and here too, DMS does not affect the intrinsic energy barrier for the reaction (see Table S5).

These results, despite being at a less reliable level of theory, strongly suggest that the DMS complexation does not lower the intrinsic barriers for unimolecular rearrangements, and might even slightly increase them. Any catalytic effect of DMS on the unimolecular decomposition of CI is then due to the energy release of the complexation, but this is insufficient to lower the decay TS close to or below the energy level of free CI + DMS, such that the main fate of the complex remains redissociation without chemical loss. For example, the net energy barrier for the DMS-catalysed *Z*-MVKO unimolecular reaction is ~ +4 kcal/mol, still implying a slow bimolecular reaction. This is in agreement with the observations of the current experimental study, which sees no enhanced CI loss in the presence of DMS.

There are many other reactions in the isoprene + O_3 system that might be catalytically enhanced or slowed by DMS, and examining all of these is outside the scope of this study. We did examine the reaction of DMS with the adduct of CH_2OO + SO_2, *i.e.* the thio-secondary ozonide (*cyc*-$CH_2OOS(O)O$-, thio-SOZ) (Kuwata et al., 2015;Vereecken et al., 2012) formed

prior to its decomposition to SO_3 + CH_2O. The DMS-catalyzed redissociation of thio-SOZ back to CH_2OO + SO_2, thus inhibiting SO_2 oxidation by CI, was found at the M06-2X/cc-pVDZ level of theory to have an energy barrier of 17.8 kcal mol^{-1}, too high to compete against SO_3 formation for which a barrier ≤ 10 kcal mol^{-1} was found (Kuwata et al., 2015). Any inhibiting effect by DMS on the CI + SO_2 reaction is thus not caused by an enhanced redissociation of the thio-SOZ intermediate.

No data is available elucidating whether bimolecular reactions of CI-DMS complexes with suitable co-reactants (SO_2, H_2O, acids,…), or alternatively DMS complexes of such co-reactants with free CI, are hindered or enhanced relative to those of the free CI + co-reactant.

Table S5: ZPE-corrected DMS complex energies, E(complex), and barrier heights E_b without and with a DMS complexing agent, at the M06-2X/cc-pVDZ level of theory. Energies are in kcal mol^{-1} and relative to the free reactants.

CI reaction	E_b	E(complex)	E_b(complex)
CH_2OO → cyc-CH_2OO-	22.0	–9.6	14.5
Z-CH_3CHOO → CH_2CHOOH	12.7	–8.6	7.2
Z-CH_3CHOO → cyc-$CH(CH_3)OO$-	25.8	–8.6	18.2
E-CH_3CHOO → cyc-$CH(CH_3)OO$-	18.4	–10.9	9.5
Z-$(CH=CH_2)C(CH_3)OO$ → cyc-CH-$CH_2C(CH_3)OO$-	12.1	–9.9	4.4
Z-$(CH=CH_2)C(CH_3)OO$ + DMS → MVK + DMSO	8.7		
E-$(CH_3)C(CH=CH_2)OO$ + DMS → MVK + DMSO	8.0		
$(CH_3)C(CH=CH_2)OO$ + DMS →$S(CH_3)(=CH_2)C(CH_3)(CH=CH_2)OOH$	11.2		

References

Kuwata, K. T., Guinn, E. J., Hermes, M. R., Fernandez, J. A., Mathison, J. M., and Huang, K.: A Computational Re-examination of the Criegee Intermediate–Sulfur Dioxide Reaction, J. Phys. Chem. A, 119, 10316-10335, 10.1021/acs.jpca.5b06565, 2015.

Limão-Vieira, P., Eden, S., Kendall, P. A., Mason, N. J., and Hoffmann, S. V.: High resolution VUV photo-absorption cross-section for dimethylsulphide, $(CH_3)_2S$, Chemical Physics Letters, 366, 343-349, https://doi.org/10.1016/S0009-2614(02)01651-2, 2002.

Lin, Y.-H., Li, Y.-L., Chao, W., Takahashi, K., and Lin, J. J.-M.: The role of the iodine-atom

adduct in the synthesis and kinetics of methyl vinyl ketone oxide—a resonance-stabilized Criegee intermediate, Phys. Chem. Chem. Phys., 22, 13603-13612, 10.1039/D0CP02085K, 2020.

Liu, C.-P., Reid, S. A., and Lee, Y.-P.: Two-color resonant four-wave mixing spectroscopy of highly predissociated levels in the $\tilde{A}^2A_1$ state of CH_3S, J. Chem. Phys., 122, 124313, 10.1063/1.1867333, 2005.

Mir, Z. S., Lewis, T. R., Onel, L., Blitz, M. A., Seakins, P. W., and Stone, D.: CH_2OO Criegee intermediate UV absorption cross-sections and kinetics of $CH_2OO + CH_2OO$ and $CH_2OO + I$ as a function of pressure, Phys. Chem. Chem. Phys., 22, 9448-9459, 10.1039/D0CP00988A, 2020.

Newland, M. J., Rickard, A. R., Vereecken, L., Muñoz, A., Ródenas, M., and Bloss, W. J.: Atmospheric isoprene ozonolysis: impacts of stabilised Criegee intermediate reactions with SO_2, H_2O and dimethyl sulfide, Atmos. Chem. Phys., 15, 9521-9536, 10.5194/acp-15-9521-2015, 2015.

Ting, W. L., Chang, C. H., Lee, Y. F., Matsui, H., Lee, Y. P., and Lin, J. J. M.: Detailed mechanism of the $CH_2I + O_2$ reaction: Yield and self-reaction of the simplest Criegee intermediate CH_2OO, J. Chem. Phys., 141, 104308, 10.1063/1.4894405, 2014.

Vereecken, L., Harder, H., and Novelli, A.: The reaction of Criegee intermediates with NO, RO_2, and SO_2, and their fate in the atmosphere, Phys. Chem. Chem. Phys., 14, 14682-14695, 10.1039/C2CP42300F, 2012.